JOURNAL OF MATERIALS SCIENCE 23 (1988) 2649–2660

Microstructural development in the oxidation-induced phase transformation of Fe–Al–Cr–Mn–C alloys

JENQ-GONG DUH, J. W. LEE, CHAUR-JENG WANG
Department of Materials Science and Engineering, National Tsing Hua University, Hsinchu, Taiwan

Electron microscopic analysis has been used to investigate the interfacial phenomena in a high-temperature alloy system. During high-temperature oxidation of Fe–8.9Al–3Cr–31Mn–0.87C alloy at 800 and 1000° C, an oxidation-induced transformation α layer was observed between the γ matrix and the oxide scale. The morphology of the oxidized sample was studied by scanning electron microscopy, and the elemental redistribution of the constituents was evaluated using an electron microprobe. The concentration of elements was detected with the ZAF-corrected quantitative program. It is believed that the formation of the α layer was caused by the selective oxidation of manganese during the oxidation process. The thickness of the α layer increased with both oxidation time and temperature, the temperature having the greater influence on this transformed layer. In addition, the interfacial concentrations at the γ/α and α/oxide boundaries were employed to investigate the selective oxidation of manganese.

1. Introduction

The Fe–Mn–Al alloy systems have good high-temperature oxidation resistance due to the presence of aluminium, and the addition of chromium leads to the formation of an α-Al_2O_3 layer by acting as an oxygen getter [1, 2], or possibly as a stabilizer of α-Al_2O_3 rather than γ-Al_2O_3 which is less protective [3]. The combination of manganese and carbon is believed to be an austenitic stabilizer which extends and stabilizes the gamma loop in iron and then retains the face centred cubic austentic phase. Several investigators have studied the high-temperature oxidation of Fe–Mn–Al alloy systems in recent years [4–12]. More recently, Duh *et al.* investigated the oxidation of Fe–31Mn–8.9Al–3Cr–0.87C alloys [13] and Fe–Mn–9.6Al–0.8C alloys with various contents of manganese [14] at 800 and 1000° C; Kao *et al.* [15] studied the alloys of Fe–xMn–yAl–zC (x = 29.6 to 34.4, y = 7.8 to 8.4, z = 0.3 to 1.3); Smolik *et al.* [16] investigated the Fe–30Mn–8Al–1C–xSi alloys (x = 0.2, 1.5); and Lopes *et al.* [17] worked on the Fe–36.47Mn–0.13C–7.38Al alloys.

In some of the oxidation work in the Fe–Al–Mn-based alloy [5, 6, 9, 11, 15, 18], it was found that a second phase with different crystalline structure existed between the alloy matrix and the oxide scales. Similar observations have been reported in Fe–Mn [19], Fe–Mn–Cr [20], and Fe–Mn–Ni–Si [21, 22] systems. The purpose of this study was to investigate the oxidation-induced phase transformation phenomena in this new Fe–Mn–Al–Cr alloy system. The morphology of the oxide scale was studied by scanning electron microscopy and the concentration profiles of the elements were evaluated using a quantitative analysis programme in an electron microprobe. The growth of the oxidation-induced transformation is discussed in terms of the diffusional interaction among the species and the interfacial topography between the metal matrix and the induced layer.

2. Experimental procedure

2.1. Alloy preparation

The alloy was prepared from electrolytic iron (99%), electrolytic manganese (99.96%), electrolytic chromium (99.92%) and high-purity aluminium (99.96%). Before melting, these raw materials were dried in a hot air furnace. The alloy was fabricated in an L-HIS 8/III vacuum melting furnace. Iron, aluminium and chromium were first loaded at about 10 mbar. Manganese and carbon were the elements to be charged last. Argon was introduced into the chamber to reduce the evaporation of manganese and carbon.

After melting, casting was performed into a steel mould at about 1600° C. The ingot was hot forged at 1200° C to reduce the thickness from 4 cm to 2.3 cm and then homogenized at 1200° C for 12 h. After surface finishing, the alloy was hot rolled at 1000° C from 20 mm to 2.5 mm in thickness. The alloy was surface finished again to avoid any impurity diffusion into the matrix. Annealing was then carried out at 1150° C for 50 h in a quartz tube with flowing argon. The compositions of the alloy were analysed by wet chemical analysis and are listed in Table I.

After these treatments, the alloy was ground to remove the oxide scales. Rectangular specimens, 10 mm × 25 mm × 2 mm in dimension, were cut from the alloy. The specimen surfaces were abraded and polished up to 0.05 μm Al_2O_3 powder, washed in

0022–2461/88 $03.00 + .12

TABLE I The compositions of the austentic alloy analysed by wet chemical analysis

	Mn	Al	Cr	C	S	Fe
wt %	30.95	8.87	2.98	0.87	0.013	Bal.

distilled water, ultrasonically degreased in acetone and rinsed in alcohol. All specimens were stored in alcohol to prevent pollution.

2.2. Oxidation

The oxidation experiment was carried out in a three-zone horizontal tube furnace (Therco/Mini Brute) at 800 and 1000° C with dried air pumped at a flow rate of 400 $cm^3 min^{-1}$. The air was dried by passing through a calcium chloride drying tube before entering the furnace. The constant temperature zone (± 3° C) for the furnace was about 16 cm long. The oxidation times for the alloy were 24, 48, 250 h at 800° C, and 9, 12, 24, 48, 120 h at 1000° C. After oxidation, the samples were furnace cooled to prevent scale spalling during cooling. Several samples were purposefully water quenched to freeze the high-temperature state for the concentration profile measurement. The detailed experimental condition is given in Table II. Two specimens were oxidized for the same condition each time. One was for electron microprobe analysis, and another for the X-ray diffraction study. A reproducibility test was also employed for each oxidation condition. The samples for microprobe analysis were cold mounted, sectioned with a diamond saw and polished to 0.05 μm Al_2O_3.

2.3. Analysis

The possible phases of the oxidized sample were identified with a Shimatzu X-ray diffractometer equipped with a copper target, nickel filter and a graphite single-crystal monochrometer.

The oxidized sample was subsequently abraded with no. 600 SiC paper from the external surface towards the matrix to reveal the different oxide scales. The overall abraded thickness was about several tens of micrometres each time.

The morphologies of the oxide and the inner layer were examined with an optical microscope (OM) and a scanning electron microscope (SEM). The elemental redistribution after oxidation was detected with an electron microprobe (Jeol JCXA-733) by quantitative analysis of the concentrations of iron, aluminium, manganese and chromium with the aid of a ZAF-corrected program. The carbon profile was analysed by the line scanning technique instead. X-ray mapping was also employed to investigate the elemental distribution. These concentration data were stored in a personal computer for further calculation and plotting usage.

TABLE II Oxidation conditions employed at 800 and 1000° C

Temperature (° C)	Time (h)
800	24*, 48*, 250*
1000	9†, 12†*, 24*, 48†, 120†

*Furnace cooled.
†Water quenched.

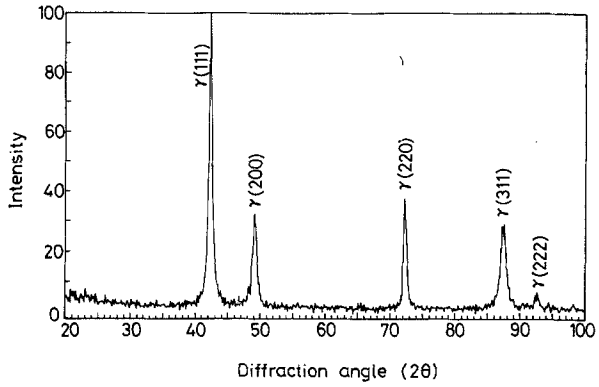

Figure 1 X-ray diffraction pattern of the austenitic matrix.

3. Results

3.1. Structure before oxidation

After the homogenization annealing process, the alloy exhibited a homogeneous pure austenitic phase based on the X-ray diffraction results, as shown in Fig. 1. The lattice parameter was calculated to be 0.367 nm.

3.2. Morphology of the oxide scale

3.2.1. Oxidation at 800° C

The morphology of the sample oxidized for 24 h is presented in Fig. 2. On the basis of the SEM images and the X-ray mapping results, it is observed that the oxide scale is manganese rich. The oxide–metal interface is rich in aluminium, which is further identified as α-Al_2O_3 from the X-ray diffraction data. The high chromium concentration in the metal–oxide interface, as indicated in Fig. 2d, corresponds to the presence of chromium carbide.

With the aid of the X-ray diffraction pattern, the phases of the external oxide scale were identified as (Fe, Mn)$_3O_4$ with some α-Fe_2O_3, which were always spalled away during cooling to room temperature. With successive abrasion of the sample surface, the internal oxide layer was found to consist of mainly (Fe, Mn)Al_2O_4 and (Fe, Cr)$_2O_3$ with a little α-Al_2O_3.

3.2.2. Oxidation at 1000° C

The morphology of the sample oxidized for 12 h was almost identical to the furnace-cooled and water-quenched conditions. From the X-ray mapping results of the samples oxidized for 12 h as presented in Fig. 3, the oxide scale was found to be rich in manganese and aluminium, while the precipitate of chromium carbide was not found. SEM images and the X-ray mapping results for the sample oxidized for 24 h are also shown in Fig. 4.

On the basis of the results from X-ray diffraction data of the samples oxidized for 12 and 24 h, the phases of the surface oxide scale were identified to be mainly Mn_3O_4 together with some Fe_3O_4. After successive abrasions, Mn_3O_4 gradually disappears, while MnO, $MnAl_2O_4$, (Fe, Cr)$_2O_3$ and α-Al_2O_3 showed up. With the aid of the overall X-ray diffraction data [12], a diagrammatic representation of the oxide scales of the sample oxidized at 1000° C is shown in Fig. 5, which gives a pictorial view of the microstructural development of the alloy during oxidation.

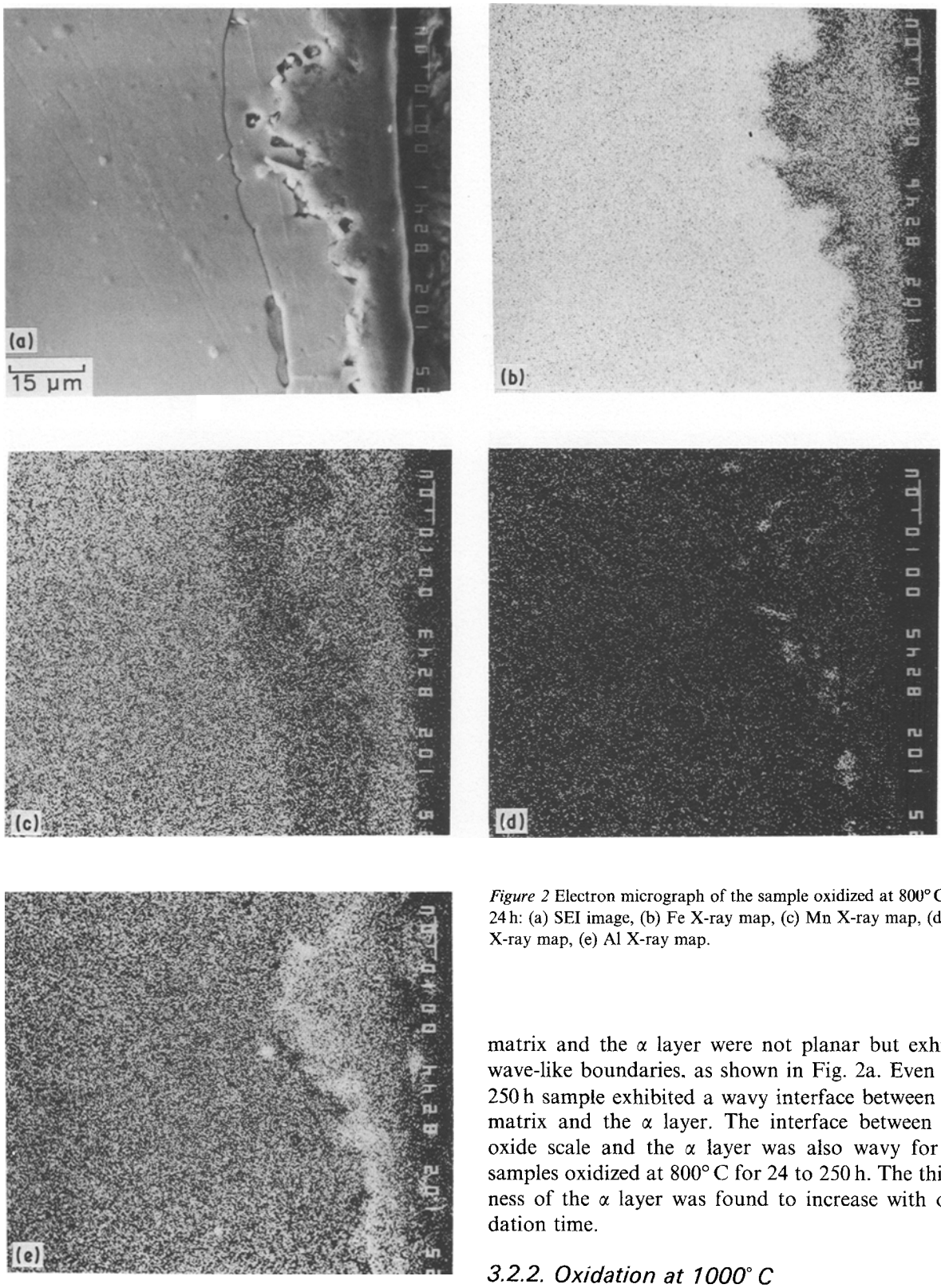

Figure 2 Electron micrograph of the sample oxidized at 800° C for 24 h: (a) SEI image, (b) Fe X-ray map, (c) Mn X-ray map, (d) Cr X-ray map, (e) Al X-ray map.

3.3. Morphology of the oxidation-induced layer

3.3.1. Oxidation at 800° C

From the pictures of the X-ray mapping of manganese and iron, as shown in Fig. 2, a concentration decrease of manganese is observed from the matrix towards the oxide scale, while an increase is found for iron. The interesting region between the matrix and the oxide scale is the oxidation-induced α layer. On the basis of the SEM images of the samples oxidized for different times at 800° C, it was found that the interfaces of the matrix and the α layer were not planar but exhibit wave-like boundaries, as shown in Fig. 2a. Even the 250 h sample exhibited a wavy interface between the matrix and the α layer. The interface between the oxide scale and the α layer was also wavy for all samples oxidized at 800° C for 24 to 250 h. The thickness of the α layer was found to increase with oxidation time.

3.2.2. Oxidation at 1000° C

The α layer can be identified from the X-ray diffraction pattern as shown in Fig. 6 for the sample oxidized for 48 h after surface abrasion.

Observation of the SEM images as shown in Figs 3a and 4a taken after 12 and 24 h oxidation, respectively, showed that the interfaces between the α layer and the matrix are all planar, while the interfaces between the oxide scale and the α layer were still wavy. On comparison with the samples oxidized at 800° C, it was obvious that the thickness of the α layer at 1000° C was much larger than that at 800° C. For the sample oxidized at 1000° C for 12 h, the layer was even wider than that oxidized at 800° C for 250 h.

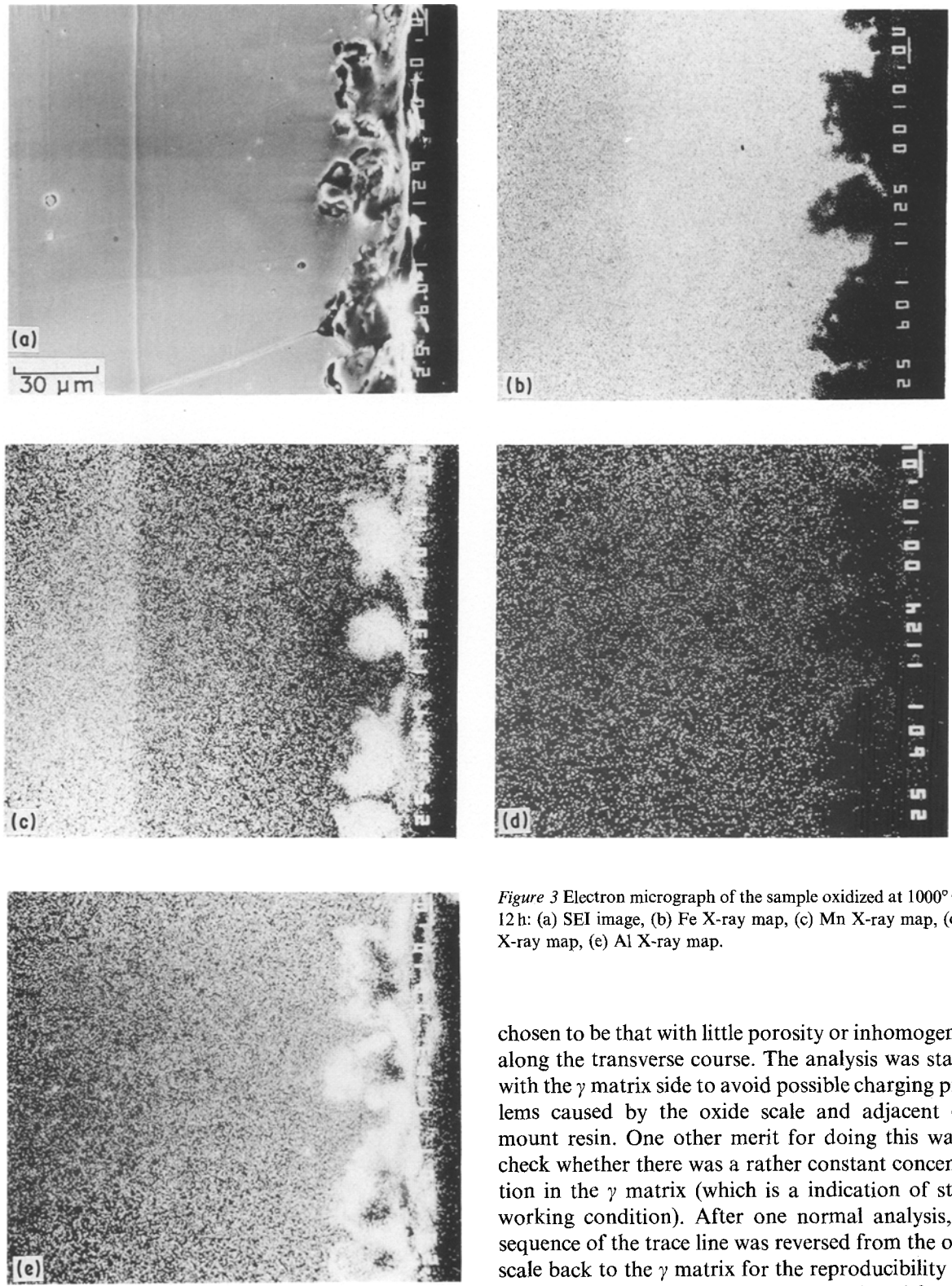

Figure 3 Electron micrograph of the sample oxidized at 1000° C for 12 h: (a) SEI image, (b) Fe X-ray map, (c) Mn X-ray map, (d) Cr X-ray map, (e) Al X-ray map.

3.4. Quantitative analysis

3.4.1. Operation conditions

The operation conditions for the quantitative analysis with the electron microprobe were as follows: accelerating voltage 25 kV, beam current 2×10^{-8} A and working distance 11 mm. In order to avoid the charging caused by the cold mount resin and also to make good electric conduction of the specimen, a thin film of gold about 10 nm thick was coated with a cool sputtering coater (Polaron E-5100).

In the quantitative analysis, the trace line was chosen to be that with little porosity or inhomogeneity along the transverse course. The analysis was started with the γ matrix side to avoid possible charging problems caused by the oxide scale and adjacent cold mount resin. One other merit for doing this was to check whether there was a rather constant concentration in the γ matrix (which is a indication of stable working condition). After one normal analysis, the sequence of the trace line was reversed from the oxide scale back to the γ matrix for the reproducibility test. In general, several trace lines were employed for each specimen.

3.4.2. Oxidation at 800° C

For samples oxidized at 800° C for 24, 48 and 250 h, the morphologies of the γ/α interface were all wave-like. In the analysis of the sample oxidized for 24 h, two trace lines, A and B, were applied, in which the curvature of the interface region between the α layer and the γ matrix was different. The widths of the α layer for trace lines A and B are estimated to be 11 and 4 μm, respectively. It was found that the concentration associated with various trace lines turned out to be nearly the same, even though the interfacial

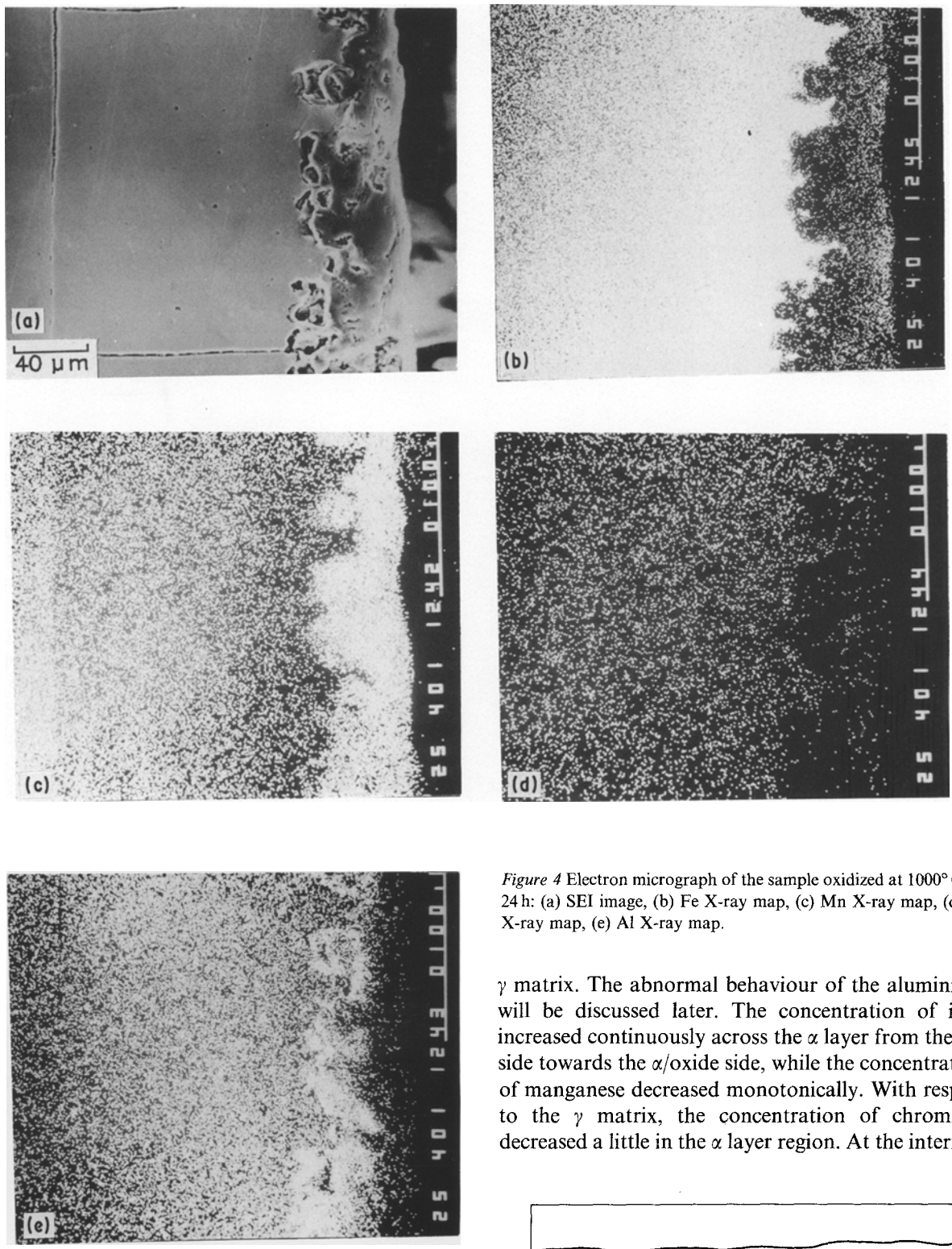

Figure 4 Electron micrograph of the sample oxidized at 1000° C for 24 h: (a) SEI image, (b) Fe X-ray map, (c) Mn X-ray map, (d) Cr X-ray map, (e) Al X-ray map.

morphologies varied. The total amount of elemental concentration was normalized to 100% in the γ matrix and the α layer, while the concentration of elements in the oxide scale was left as the raw data. The concentration profiles for oxidation at 24, 48 and 250 h are shown in Figs 7 to 9 respectively.

For an oxidation of 250 h, the concentration of each element was almost constant in the γ matrix. At the interface of the γ–α boundary there was a concentration drop for aluminium and manganese from the γ side towards the α side, while the concentration of iron increased. Within the α layer region, the concentration of aluminium bounced to a level below that in the γ matrix. The abnormal behaviour of the aluminium will be discussed later. The concentration of iron increased continuously across the α layer from the γ/α side towards the α/oxide side, while the concentration of manganese decreased monotonically. With respect to the γ matrix, the concentration of chromium decreased a little in the α layer region. At the interface

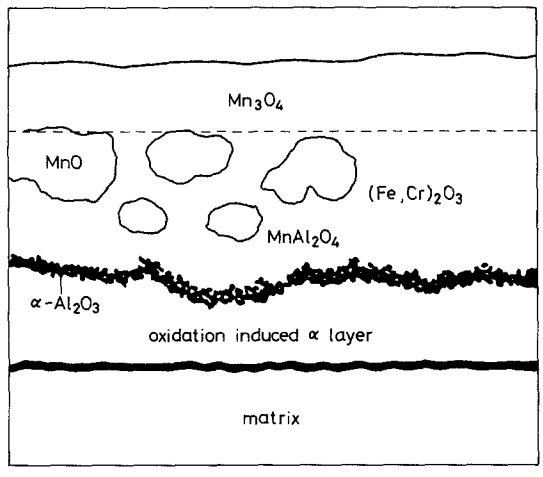

Figure 5 Diagrammatic representation of the oxide scale of the alloy oxidized at 1000° C.

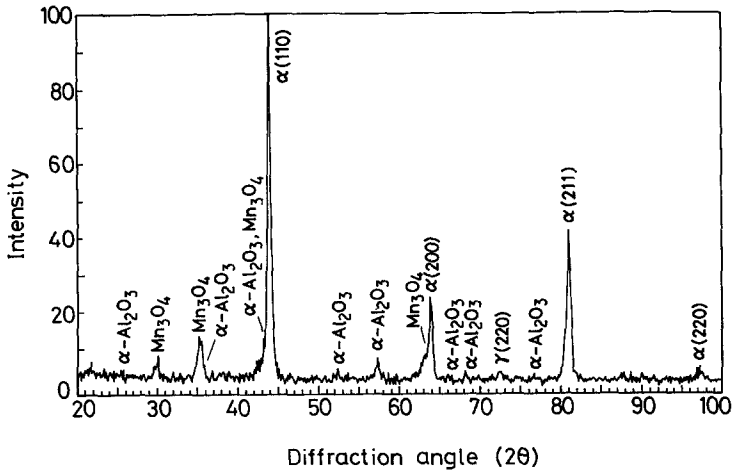

Figure 6 X-ray diffraction pattern of the α layer and some inner oxides formed at 1000° C for 48 h after abrasion.

between the α layer and the oxide scale, there was a dramatic increase in the concentration of aluminium, which is believed to be the α-Al_2O_3 layer and some aluminium-containing oxides. A local enrichment for the concentration of chromium existed around this region where the chromium carbides precipitated.

Within the oxide scale region, there was local enhancement of the iron, manganese and aluminium concentrations, as shown in Fig. 9, which was considered to be the (Mn, Fe)Al_2O_4 oxides in these localized regions. In the region about 90 μm away from the γ–α interface, there was enrichment of iron and chromium, where the $(Fe, Cr)_2O_3$ was formed.

In order to gain a better understanding concerning the movement of each species during oxidation, a detailed quantitative analysis for elements iron, manganese, aluminium and chromium is carried out around the interfacial region of γ/α and γ/oxide. The analysis scheme was performed by automatically shifting the sample stage in the electron microprobe every 1 μm around the interface region. The resulting interfacial compositions at both the γ/α and α/oxide interfaces are presented in Table III for oxidations of 24, 48 and 250 h. Also listed in Table III are the manganese concentration gradients across the α layer. The implication of the manganese concentration gradients will be investigated.

3.4.3. Oxidation at 1000° C

For samples oxidized at 1000° C, the planar interfaces between the γ matrix and the α layer region were always observed when the oxidation time was longer than 9 h. Because of the nature of the wave-like interfaces between α and oxide scale, quantitative analysis of the elemental concentration was carried out with respect to the morphologies of samples oxidized for various times. There are three trace lines, A, B and C, in the analysis for the sample oxidized at 1000° C for 12 h in order to elucidate the concentration change due to the different widths of the layer. The concentration profiles of the sample oxidized for 12, 24, 48 and 120 h are presented in Figs 10 to 13, respectively. The analysis scheme is the same as that in the case of 800° C oxidation.

After oxidation for 120 h, the concentration of each element was essentially constant in the γ matrix. At the γ–α interface, there was a drop of concentration for both aluminium and manganese, while the concentration of iron increased. Within the α region, the concentration of iron rose from the γ/α side towards the α/oxide side, while the concentration of manganese decreased continuously. The amount of aluminium increased to a level above that in the γ matrix. The concentration of chromium increased somewhat in the α layer region, which is different from the case

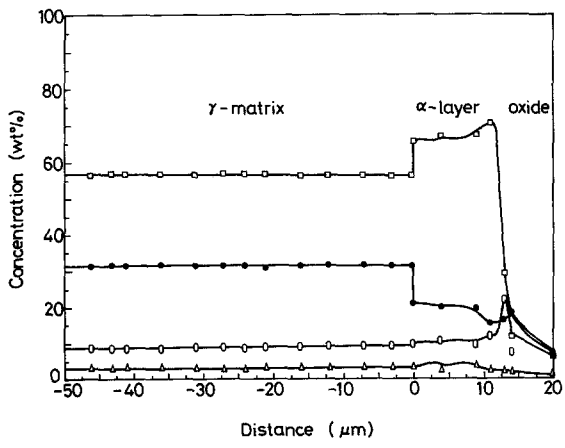

Figure 7 Concentration profiles of the sample oxidized at 800° C for 24 h. (□) Fe, (●) Mn, (△) Cr, (○) Al.

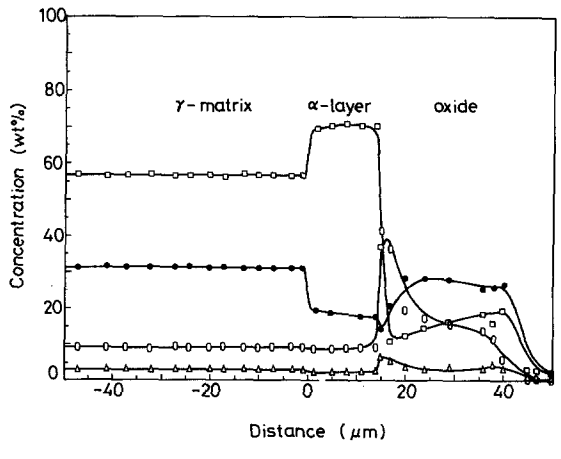

Figure 8 Concentration profiles of the sample oxidized at 800° C for 48 h. (□) Fe, (●) Mn, (△) Cr, (○) Al.

TABLE III Interfacial concentration for the alloy oxidized at 800° C

Time (h)	α layer thickness (μm)	α/γ interface	Fe (wt %)			Mn (wt %)			Cr (wt %)			Al (wt %)			$\frac{\partial C^{*}_{Mn}}{\partial x}$ (wt % μm^{-1})
			$C^{\gamma,\gamma/\alpha}_{Fe}$	$C^{\alpha,\gamma/\alpha}_{Fe}$	$C^{\alpha,\alpha/o}_{Fe}$	$C^{\gamma,\gamma/\alpha}_{Mn}$	$C^{\alpha,\gamma/\alpha}_{Mn}$	$C^{\alpha,\alpha/o}_{Mn}$	$C^{\gamma,\gamma/\alpha}_{Cr}$	$C^{\alpha,\gamma/\alpha}_{Cr}$	$C^{\alpha,\alpha/o}_{Cr}$	$C^{\gamma,\gamma/\alpha}_{Al}$	$C^{\alpha,\gamma/\alpha}_{Al}$	$C^{\alpha,\alpha/o}_{Al}$	
24 (trace line A)	11	NP†	56.4	65.7	70.6	31.3	20.9	15.3	3.1	3.2	2.3	9.2	10.2	11.8	−0.51
24 (trace line B)	4	NP	56.7	64.6	68.9	31.0	21.3	19.2	3.1	2.7	2.6	9.3	11.4	9.3	−0.53
48	14	NP	56.6	69.3	70.7	31.0	19.6	17.7	3.1	2.4	2.4	9.3	8.7	9.2	−0.14
250	51	NP	56.9	71.3	73.7	31.1	18.1	14.2	3.0	2.5	2.5	9.0	8 1	9.6	−0.08

*$\partial C_{Mn}/\partial x$ indicates the average concentration gradient from α/γ interface through the α layer to the α/o interface.
†NP: nonplanar interface.
γ/α represents the γ matrix and α layer interface.
α/o represents the α layer and oxide scale interface.

TABLE IV Interfacial concentration for the alloy oxidized at 1000° C for 12 h

Trace line	α layer thickness (μm)	α/γ interface	Fe (wt %)			Mn (wt %)			Cr (wt %)			Al (wt %)			$\frac{\partial C_{Mn}}{\partial x}$ (wt % μm^{-1})
			$C^{\gamma,\gamma/\alpha}_{Fe}$	$C^{\alpha,\gamma/\alpha}_{Fe}$	$C^{\alpha,\alpha/o}_{Fe}$	$C^{\gamma,\gamma/\alpha}_{Mn}$	$C^{\alpha,\gamma/\alpha}_{Mn}$	$C^{\alpha,\alpha/o}_{Mn}$	$C^{\gamma,\gamma/\alpha}_{Cr}$	$C^{\alpha,\gamma/\alpha}_{Cr}$	$C^{\alpha,\alpha/o}_{Cr}$	$C^{\gamma,\gamma/\alpha}_{Al}$	$C^{\alpha,\gamma/\alpha}_{Al}$	$C^{\alpha,\alpha/o}_{Al}$	
A	80	P†	56.7	69.0	79.0	31.3	18.0	7.1	3.0	3.7	4.1	9.0	9.3	9.8	−0.14
B	87	P	57	68.5	82.1	31.1	18.7	5.2	3.0	3.6	4.2	9.0	9.3	9.6	−0.16
C	80	P	56.8	69.3	80.4	31.2	18.0	5.6	3.0	3.6	4.2	9.0	9.1	9.8	−0.16

†P: planar interface.

TABLE V Summary of interfacial concentration for the alloy oxidized at 1000° C

Time (h)	α layer thickness (μm)	γ/α interface	Fe (wt %)			Mn (wt %)			Cr (wt %)			Al (wt %)			$\frac{\partial C_{Mn}}{\partial x}$ (wt % μm^{-1})
			$C^{\gamma,\gamma/\alpha}_{Fe}$	$C^{\alpha,\gamma/\alpha}_{Fe}$	$C^{\alpha,\alpha/o}_{Fe}$	$C^{\gamma,\gamma/\alpha}_{Mn}$	$C^{\alpha,\gamma/\alpha}_{Mn}$	$C^{\alpha,\alpha/o}_{Mn}$	$C^{\gamma,\gamma/\alpha}_{Cr}$	$C^{\alpha,\gamma/\alpha}_{Cr}$	$C^{\alpha,\alpha/o}_{Cr}$	$C^{\gamma,\gamma/\alpha}_{Al}$	$C^{\alpha,\gamma/\alpha}_{Al}$	$C^{\alpha,\alpha/o}_{Al}$	
12	82 ± 3	P	56.8 ±0.1	68.9 ±0.4	80.5 ±1.2	31.3 ±0.1	18.2 ±0.4	6.0 ±0.7	3.0	3.5 ±0.1	4.2 ±0.1	9.0	9.2 ±0.1	9.7 ±0.1	−0.15
24	149 ± 6	P	56.6	68.6 ±0.8	77.1 ±1.5	31.3 ±0.1	18.1 ±0.7	8.7 ±1.5	3.1	3.7 ±0.1	4.1 ±0.1	9.1	9.6	9.8 ±0.3	−0.065
48	174 ± 7	P	57.15 ±0.5	71.5 ±0.4	76.8 ±0.1	30.2 ±0.2	15.5 ±0.3	9.6 ±0.6	3.1	3.8	4.0 ±0.1	9.0 ±0.1	9.3	9.7 ±0.3	−0.03
120	231 ± 19	P	61.3 ±0.1	70.4 ±0.3	74.0 ±1.3	26.95 ±0.15	16.5 ±0.3	13 ±1.8	3.1	3.8 ±0.2	3.75 ±0.05	8.65 ±0.05	9.4 ±0.2	9.3 ±0.1	−0.015

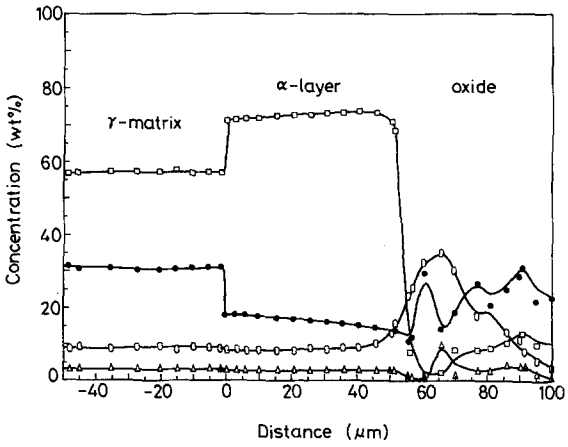

Figure 9 Concentration profiles of the sample oxidized at 800° C for 250 h. (□) Fe, (●) Mn, (△) Cr, (○) Al.

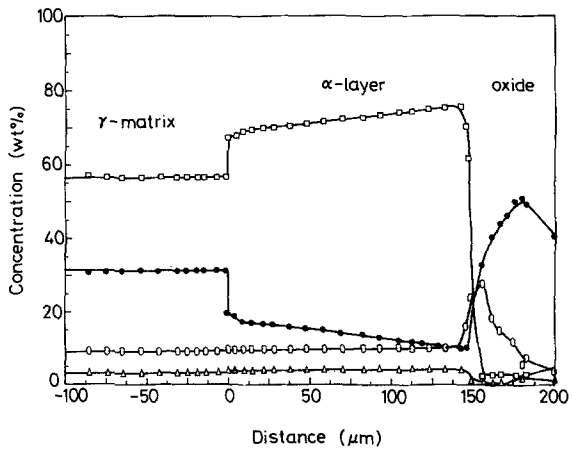

Figure 11 Concentration profiles of the sample oxidized at 1000° C for 24 h. (□) Fe, (●) Mn, (△) Cr, (○) Al.

for oxidation at 800° C. At the interface between the α layer and the oxide scale, the concentration of aluminium increased rapidly where the α-Al_2O_3 layer and some aluminium-containing oxides were formed. Within the oxide scale, there were increases of manganese and aluminium, which are believed to be the oxide of the $MnAl_2O_4$. Near the outside of the oxide scale, the concentrations of iron and chromium rose due to the formation of $(Fe, Cr)_2O_3$ oxides. On the outermost side of the oxide scale, only manganese was detected where the Mn_3O_4 was formed.

The interfacial composition for each element was evaluated in the same way as that for 800° C oxidation. Table IV lists the interfacial compositions for 12 h oxidation with respect to various trace line analysis. A summary of the data for different oxidation times is presented in Table V.

4. Discussion

4.1. Influential factors in the quantitative analysis

4.1.1. Coating effect

The advantages of the gold coating on the oxidized sample for quantitative analysis have been stated in Section 3. A further advantage of the coating is the resulting stable working conditions during analysis. It was observed that the position of the uncoated sample in the sample stage of the microprobe shifted about several tens of micrometres after analysis, while the coated sample did not. It is believed that the heat produced by the electron beam bombardment on the sample will be conducted away quickly for the coated sample. However, for the uncoated sample, such heat might make the cold mount resin strained.

The extent of electron-beam heating can be estimated from the formula provided by Reed [23]

$$\Delta T = 4.8E_0 i/kd_p \quad (1)$$

where ΔT is the temperature rise (° C) in the specimen at the point of impact of the electron beam, E_0 is the operating voltage in kV, i is the beam current (μA), k is the thermal conductivity, ($W\,cm^{-1}\,°C^{-1}$), and d_p is the probe diameter (μm). In this Fe–Mn–Al alloy system, the temperature rises about 5° C for $k \simeq 0.7$, which would not introduce any significant effect on the quantitative analysis.

4.1.2. Etching effect

During quantitative analysis, it was found that the concentration of aluminium first dropped in the γ/α interface and then regained its value as the in the γ matrix. For other elements there was no such jumping behaviour. After many analyses, it was found that the abnormal jump in the aluminium concentration

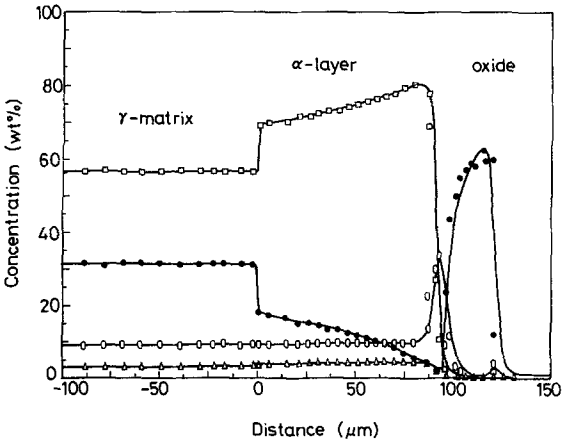

Figure 10 Concentration profiles of the sample oxidized at 1000° C for 12 h. (□) Fe, (●) Mn, (△) Cr, (○) Al.

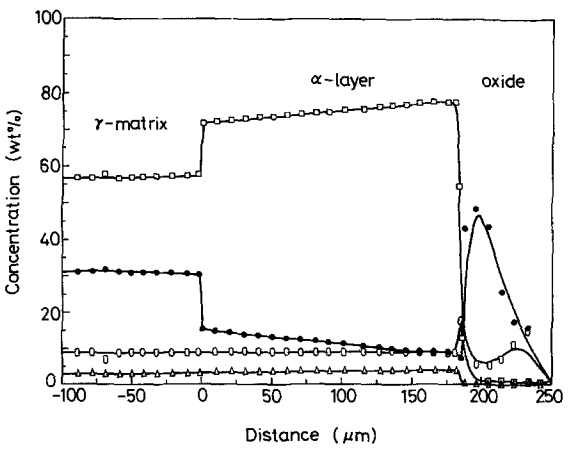

Figure 12 Concentration profiles of the sample oxidized at 1000° C for 48 h. (□) Fe, (●) Mn, (△) Cr, (○) Al.

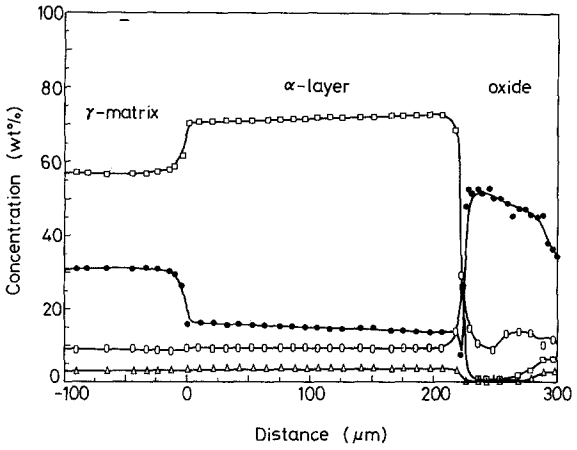

Figure 13 Concentration profiles of the sample oxidized at 1000° C for 120 h. (□) Fe, (●) Mn, (△) Cr, (○) Al.

occurred when there was a fissure in the γ/α interface. Fig. 14 shows the line profile of aluminium near the interface. There is a drop of aluminium content for the cracked interface, as seen in Fig. 14a. However, no drop of aluminium is observed for the uncracked interface, as shown in Fig. 14b. The error due to the magnitude of the surface effect on analysis precision was estimated by Yakowitz [24]. It was reported that the softer the X-ray line of interest, the worse the possible effect of a non-flat specimen examined at a given voltage would be.

4.2. The formation of the α layer

For the initial stage of oxidation, it was believed that manganese and iron had greater mobility than aluminium and chromium. It was reported that at 800° C the dissociation pressure of Mn_2O_3 was six orders of magnitude greater than that of Fe_2O_3, hence there was a significant thermodynamic driving force for the formation of a layer of Mn_2O_3 outside the Fe_2O_3 [19]. This is consistent with the experimental observation in this study that an external layer of Mn_3O_4 exists at 1000° C. Therefore, the oxidation of the alloy becomes selective for manganese rather than other base metals. Because of the effect of manganese on the stability of the austenitic phase in Fe–Mn–Al–Cr alloys, the selective oxidation of manganese would cause the transformation of the alloy matrix from the face centred cubic (fcc) γ phase to body centred cubic (bcc) α phase. This kind of oxidation-induced phase transformation has been reported in other alloy systems [19–22].

In the Fe–Mn–Al–Cr base alloy, carbon also stabilizes the austenitic structure. During oxidation, the phenomenon of decarburization could be observed for the initial stage. Nevertheless, no α layer was found in the decarburized layer for the sample oxidized at 800° C for 3 h as shown in Fig. 15. In order to distinguish the roles of manganese and carbon in the oxidation-induced transformation layer, the line profiles of carbon and manganese were detected for the sample oxidized at 1000° C for 12 h with the electron microprobe as shown in Fig. 16. It was found that the manganese concentration decreased monotonically within the α layer towards the oxide layer, which clearly indicates manganese depletion caused by oxidation. A build up of carbon was observed near the γ/α interface, while there was no signifiant change in the carbon concentration throughout the remaining regions of the α layer. The depletion of manganese across the α layer can be appreciated with the aid of Figs 17 and 18, which indicate that the manganese concentrations change dramatically from the γ matrix to the α layer for the samples oxidized at 800 and 1000° C for different times.

As the solubility of carbon is low in the α phase, the excess amount of carbon originally dissolved in γ phase is ejected from the α layer due to the removal of manganese during oxidation. The movement of carbon is diffusion-related and thus spatially dependent. It is more difficult for carbon to diffuse outward through the wide range of α layer. Instead it moves toward the γ phase and hence the carbon concentration builds up around the γ/α interface region as observed in Fig. 16, or alternatively forms the carbides within the α layer. Fig. 19, the optical micrograph of the sample oxidized at 1000° C for 120 h, indicates the latter condition.

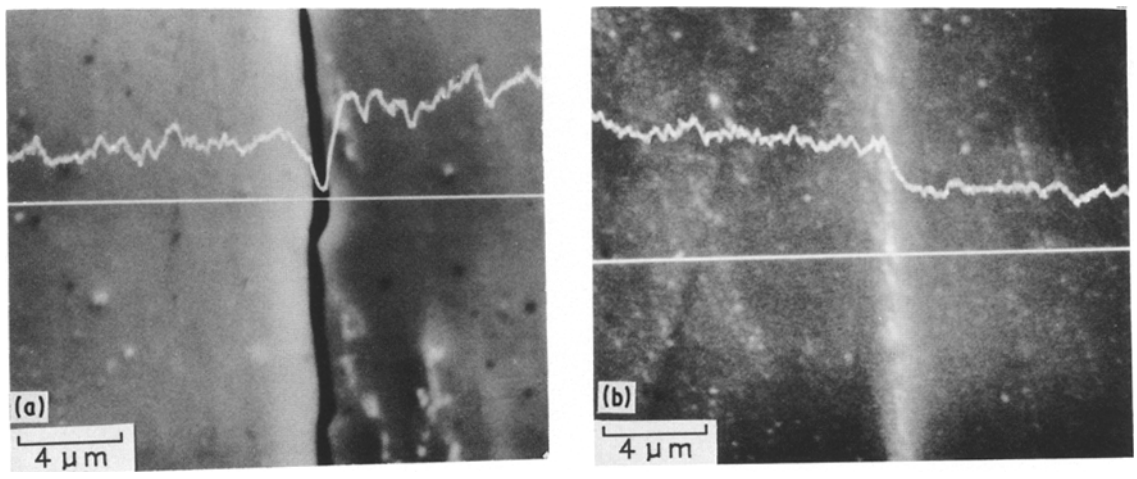

Figure 14 The line profile of aluminium near the γ/α interface, (a) for sample oxidized at 800° C for 250 h, crack visible at the interface, (b) for sample oxidized at 1000° C for 120 h, no crack observed at the interface.

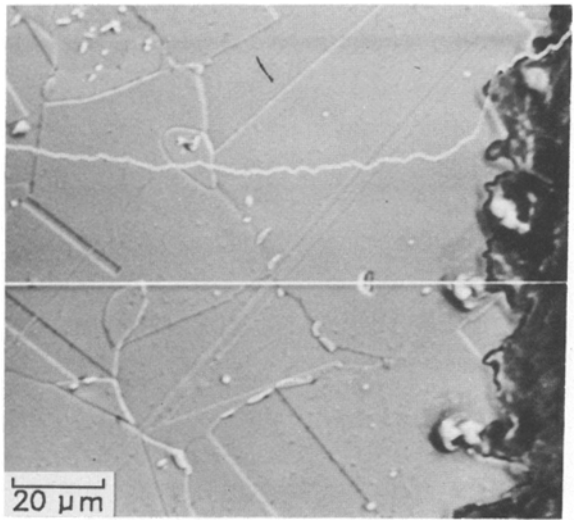

Figure 15 The line profile of carbon for the sample oxidized at 800° C for 3 h.

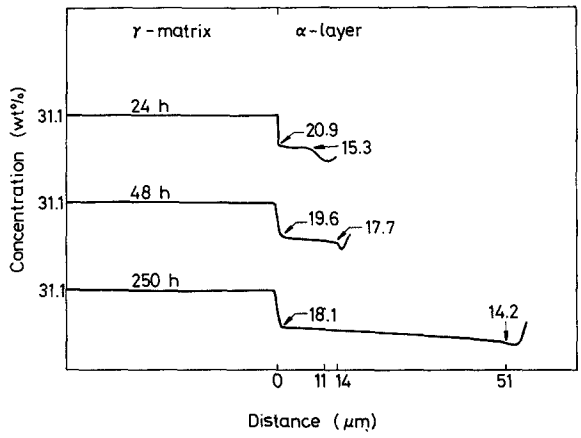

Figure 17 Concentration profiles of manganese for the samples oxidized at 800° C.

4.3. Effect of oxidation temperature and time on the growth of the α layer

From SEM observation, the morphologies of the interfaces between the α layer and the γ matrix were seen to be all wave-like for the samples oxidized at 800° C for 24, 48 and 250 h. As the oxidation time reached 250 h, the nonplanar morphology of the interface tended to smooth out. For samples oxidized at 1000° C for longer than 9 h, the γ/α interface appeared to be planar for oxidation times of 12, 24, 48, and 120 h. The thickness of the α layer for specimens oxidized at 800 and 1000° C is presented in Fig. 20 as a function of oxidation time. The layer thickness increases with increasing oxidation temperature for the same oxidation time, and it also increases with the increasing oxidation time for the same oxidation temperature. It appears that the α layer grows as the time increases, which implies a possibly diffusion-controlled process.

The thickness of the α layer for the sample oxidized at 1000° C for 24 h is estimated to be 150 μm, which is almost 20 times larger than that oxidized at 800° C for 24 h. It is apparent that temperature plays a significant role in the growth of the oxidation-induced transformation layer. From the interfacial concentration data presented in Tables III and V, it is observed that $C_{Mn}^{\alpha,\gamma/\alpha}$, the concentration of manganese at the α side of the γ/α interface, decreases as oxidation time increases, while $C_{Mn}^{\alpha,\alpha/o}$, the manganese concentration at the α side of the α/oxide interface, increases as the oxidation time increases. Because the concentration at the γ side of the interface, $C_{Mn}^{\gamma,\gamma/\alpha}$, is almost identical for 24, 48, 250 h at 800° C and also for 12, 24, and 48 h at 1000° C, the decrease of $C_{Mn}^{\alpha,\gamma/\alpha}$ indicates that more manganese is driven away through the α layer towards the oxide scale as the oxidation time increases. An abnormal increase of $C_{Mn}^{\alpha,\gamma/\alpha}$ is observed for the sample oxidized at 1000° C for 120 h. It is proposed that the concentration jump results from the slower removal of manganese due to the formation of a dense protective α-Al_2O_3 layer in the innermost region of the oxide scales.

The concentration gradient of manganese within the α layer could be evaluated from the difference of the interfacial concentration between $C_{Mn}^{\alpha,\gamma/\alpha}$ and $C_{Mn}^{\alpha,\alpha/o}$ divided by the width of the α layer. These values are also listed in Tables III and V. For oxidation at both 800 and 1000° C, the manganese concentration gradient becomes smaller as the oxidation time increases. In other words, the manganese concentration profile tends to be flat out as the oxidation progresses. This implies that a diffusion controlled mechanism might

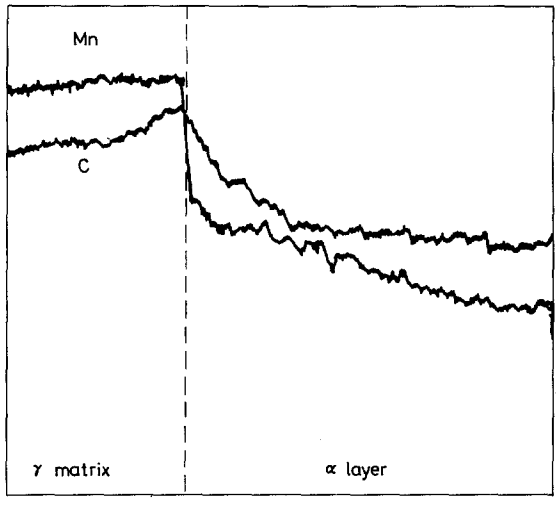

Figure 16 The line profiles of manganese and carbon for the sample oxidized at 1000° C for 12 h.

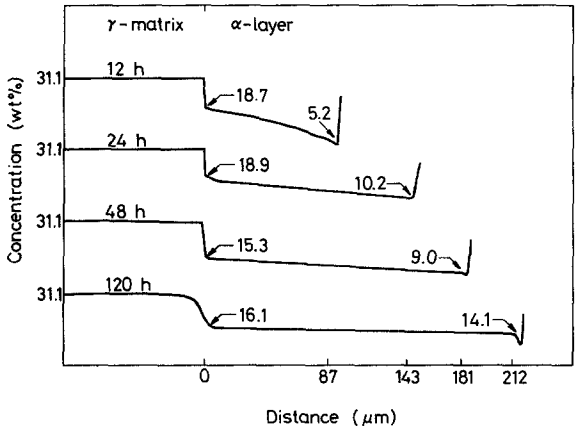

Figure 18 Concentration profiles of manganese for the samples oxidized at 1000° C.

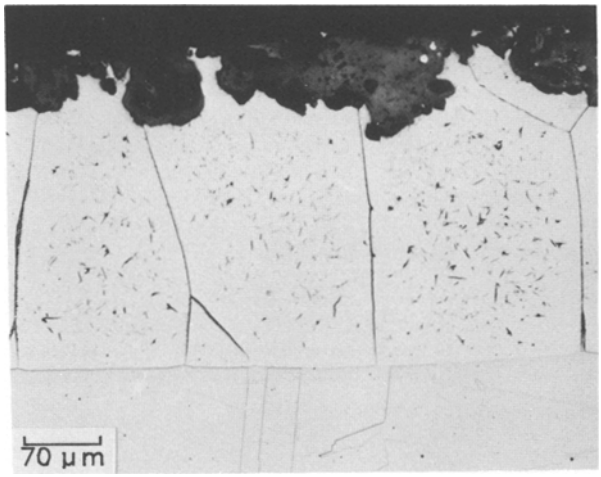

Figure 19 Optical micrograph of the sample oxidized at 1000° C for 120 h; carbides precipitated within the α layer.

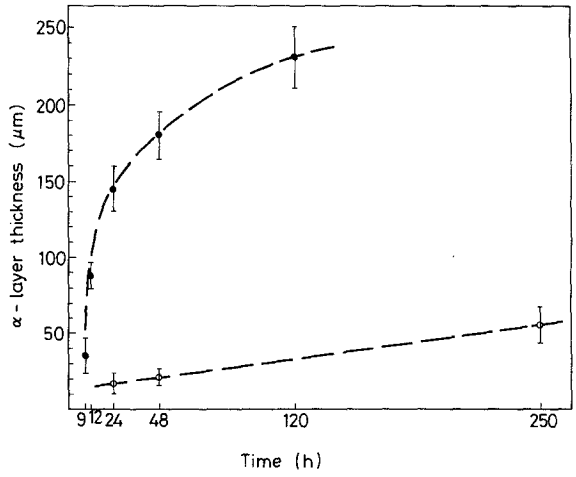

Figure 20 The thickness of the α layer for the samples oxidized at (○) 800 and (●) 1000° C.

operate during the oxidation-induced transformation. In general, the diffusion process is dependent on the temperature and time. Based on the results as indicated in Table V, the concentration gradient of manganese for a specimen oxidized at 1000° C for 12 h is 0.15 wt % μm^{-1}. The same concentration gradient is observed for a specimen oxidized at 800° C for 48 h. It appears that the oxidation temperature has more effect on the oxidation-induced transformation compared to the oxidation time.

4.4. Surface roughness effect

It is interesting to note that a localized nonplanar γ/α interface might sometimes develop at 1000° C oxidation in the reproducibility test. It is believed that the wavy interfaces result from the surface roughness during polishing treatment before oxidation. Douglass *et al.* [20] reported that there was a great difference in the rate constants of over four orders of magnitude between the electro-polished samples ($4.0 \times 10^{-9} g^2 cm^{-4} sec^{-1}$) and the abraded samples ($1.6 \times 10^{-13} g^2 cm^{-4} sec^{-1}$) at 750° C. The much slower oxidation rate of the latter could be attributed to greatly enhanced manganese diffusion through the high dislocation density, cold worked layer, and thus the protective Mn_2O_3 layer was formed outside. It was also pointed out that for the faceted surface morphology, the scale growth was limited by the slow arrival of oxidant molecules [25].

For the surface with some scratches produced during the improper polishing, the selective oxidation of manganese is somewhat less time consuming than that with a scratchless clean and smooth surface. It is argued that the nonplanar morphology of the oxidation-induced transformation layer is caused by the time delay of the removal of manganese.

5. Conclusions

1. Electron microscopic analysis technique was applied to investigate the interfacial phenomena in the Fe–8.9Al–3Cr–31Mn–0.87C alloy system.

2. An oxidation-induced transformation α layer was formed between γ matrix and oxide scales during high temperature oxidation of the alloys at 800 and 1000° C.

3. The morphology of the γ/α interface was planar for the samples oxidized at 1000° C for 12, 24, 48, 120 h, while it was nonplanar for samples oxidized at 800° C.

4. The formation of the α layer is caused by the selective oxidation of manganese at 800 and 1000° C.

5. The elemental redistribution was quantitatively analysed by the electron microprobe and the interfacial concentrations at γ/α and α/oxide were employed to probe the selective oxidation of manganese.

6. The oxidation temperature played a more important role in the oxidation-induced phase transformation than the oxidation time.

Acknowledgement

The authors wish to thank the National Science Council, Taiwan, for financial support under the contract no. NSC 76-0405-E007-11.

References

1. C. WAGNER, *J. Electrochem. Soc.* **103** (1956) 627.
2. *Idem, Corros. Sci.* **5** (1965) 751.
3. W. C. HAGEL, *Corrosion* **21** (1965) 316.
4. S. K. BANERJI, "A Update on Fe–Mn–Al Steels", Proceedings of the Workshop on "Conservation and Substitution Technology for Materials", Vanderbilt University, Nashville, TN, June 1981.
5. J. P. SAUER, R. A. RAPP and J. P. HIRTH, *Oxid. Metals* **18** (1982) 285.
6. P. R. S. JACKSON and G. R. WALLWORK, *ibid.* **21** (1984) 135.
7. H. ERHART, R. WANG and R. A. RAPP, *ibid.* **21** (1984) 81.
8. R. WANG, M. J. STRASZHEIM and R. A. RAPP, *ibid.* **21** (1984) 71.
9. B. K. LEE, Master Thesis, National Tsing Hua University, Taiwan (May 1983).
10. C. H. KAO, Master Thesis, National Tsing Hua University, Taiwan (May 1983).
11. C. J. LIN, Master Thesis, National Tsing Hua University, Taiwan (May 1984).
12. C. J. WANG, Master Thesis, National Tsing Hua University, Taiwan (May 1984).
13. J. G. DUH, C. J. WANG, C. M. WAN and B. S. CHIOU, in "Alternate Alloying for Environmental Resistance", edited by G. R. Smolik and S. K. Banerji (The

Metallurgical Society, Warrendale, Pennsylvania, 1987) p. 291.
14. J. G. DUH, C. J. LIN, J. W. LEE and C. M. WAN, *ibid.*, p. 283.
15. C. H. KAO, C. M. WAN and M. T. JAHN, *ibid.*, p. 299.
16. G. R. SMOLIK, J. E. FLINN, D. V. MILEY and G. E. KORTH, *ibid.*, p. 307.
17. M. F. S. LOPES and F. C. R. ASSUNCAO, *ibid.*, p. 231.
18. W. S. YANG, Master Thesis, National Tsing Hua University, Taiwan (May 1986).
19. P. R. S. JACKSON and G. R. WALLWORK, *Oxid. Metals* **20** (1983) 1.
20. D. L. DOUGLASS, F. GESMUNDO and C. de ASMUNDIS, *ibid.* **25** (1986) 235.
21. J. M. OH, M. J. McNALLAN and W. E. KING, *J. Electrochem. Soc.* **133** (1986) 1042.
22. J. M. OH and M. J. McNALLAN, *ibid.* **134** (1987) 1010.
23. S. J. B. REED, in "Microprobe Analysis", edited by C. A. Anderson (Wiley, New York, 1973).
24. H. YAKOWITZ, in "Fifty Years of Progress in Metallographic Techniques", ASTM-STP 430 (American Society for Testing Materials, Philadelphia, Pennsylvania, 1968) p. 383.
25. A. RAHMEL, G. C. WOOD, P. KOFSTAD and D. L. DOUGLASS, *Oxid. Metals* **23** (1985) 251.

Received 22 August
and accepted 1 December 1987